Contents lists available at ScienceDirect

Current Research in Structural Biology

Cyclohexyl-α maltoside as a highly efficient tool for membrane protein studies

Julie Winkel Missel [a], Nina Salustros [a], Eva Ramos Becares [a], Jonas Hyld Steffen [a], Amalie Gerdt Laursen [a], Angelica Struve Garcia [b], Maria M. Garcia-Alai [b,c], Čeněk Kolar [d], Pontus Gourdon [a,e], Kamil Gotfryd [a,*]

[a] *Department of Biomedical Sciences, Copenhagen University, Maersk Tower 7-9, Nørre Allé 14, DK-2200, Copenhagen N, Denmark*
[b] *European Molecular Biology Laboratory Hamburg, Notkestrasse 85, D-22607, Hamburg, Germany*
[c] *Centre for Structural Systems Biology, Notkestrasse 85, D-22607, Hamburg, Germany*
[d] *Glycon Biochemicals GmbH, Im Biotechnologie Park TGZ 1, D-14943, Luckenwalde, Germany*
[e] *Department of Experimental Medical Science, Lund University, Sölvegatan 19, SE-221 84, Lund, Sweden*

ARTICLE INFO

ABSTRACT

Membrane proteins (MPs) constitute a large fraction of the proteome, but exhibit physicochemical characteristics that impose challenges for successful sample production crucial for subsequent biophysical studies. In particular, MPs have to be extracted from the membranes in a stable form. Reconstitution into detergent micelles represents the most common procedure in recovering MPs for subsequent analysis. n-dodecyl-β-D-maltoside (DDM) remains one of the most popular conventional detergents used in production of MPs. Here we characterize the novel DDM analogue 4-trans-(4-trans-propylcyclohexyl)-cyclohexyl α-maltoside (t-PCCαM), possessing a substantially lower critical micelle concentration (CMC) than the parental compound that represents an attractive feature when handling MPs. Using three different types of MPs of human and prokaryotic origin, *i.e.*, a channel, a primary and a secondary active transporter, expressed in yeast and bacterial host systems, respectively, we investigate the performance of t-PCCαM in solubilization and affinity purification together with its capacity to preserve native fold and activity. Strikingly, t-PCCαM displays favorable behavior in extracting and stabilizing the three selected targets. Importantly, t-PCCαM promoted extraction of properly folded protein, enhanced thermostability and provided negatively-stained electron microscopy samples of promising quality. All-in-all, t-PCCαM emerges as competitive surfactant applicable to a broad portfolio of challenging MPs for downstream structure-function analysis.

1. Introduction

Membrane proteins (MPs) exert functions fundamental for cell physiology and, when dysregulated, contribute to disease progression (Cournia et al., 2015; Kulandaisamy et al., 2019). Although MPs account for 20–30% of the proteins encoded by sequenced genomes (Almen et al., 2009) and constitute 60% of all human drug targets (Tiefenauer and Demarche, 2012), the progress with deciphering high-resolution 3-D structures of MPs is rather slow (Moraes et al., 2014) and hence they remain significantly underrepresented in the RCSB Protein Data Bank (https://www.rcsb.org/) (Berman et al., 2000). Most of the reported MP structures were determined using X-ray crystallography however the current progress in the cryo-electron microscopy (cryo-EM) has yielded a growing number of entries, many of which match the resolution of the crystal structures (Cheng, 2015, 2018).

MPs are notoriously challenging to overproduce and isolate in a chemically and conformationally homogeneous form, significantly hindering structure-function characterization efforts (Junge et al., 2008; Pandey et al., 2016). One of the greatest obstacles within the MP structural biology field is to obtain samples in the necessary quality and quantity, largely reflected by the difficulties in extracting target proteins from the lipid bilayer environment and preserving stability *in vitro* (Kotov et al., 2019). The most frequently used compounds in biochemical studies of MPs are surfactants, mainly due to their amphipathic nature, exhibiting ability to solubilize lipid bilayers, and to maintain MPs in solution during purification and structural determination (Anandan and Vrielink,

---

2016). Based on the nature of the hydrophilic headgroups, detergents are divided into three major classes, *i.e.*, ionic, zwitter-ionic and non-ionic (Seddon et al., 2004). Due to charged headgroups, ionic detergents (*e.g.*, sodium dodecyl sulfate, SDS) are capable of disrupting protein-protein interactions and can display denaturing properties detrimental for protein activity (Moraes et al., 2014). The zwitter-ionic detergents share properties with the ionic detergents, but since their head group has a net charge of zero, they are considered less harsh and thus more suitable for biophysical applications, *e.g.*, nuclear magnetic resonance (NMR) spectroscopy where they are frequently used (Sim et al., 2017). In contrast, non-ionic detergents are milder and represent the subfamily of surfactants most commonly utilized in MP studies (Moraes et al., 2014; Stetsenko and Guskov, 2017).

Among other parameters, detergent selection should consider solubilization efficacy and the effects on protein stability. Moreover, the size of formed micelles is important, dictating the overall size of protein-detergent complexes that can be vital for the downstream applications, *e.g.*, crystallization (Prive, 2007; Tate, 2010) or cryo-EM (Thonghin et al., 2018). The length and composition of the alkyl chain highly affect the properties of the detergent, including the critical micelle concentration (CMC). Typically, longer chain non-ionic detergents such as n-dodecyl-β-D-maltoside (DDM), 2,2-didecylpropane-1,3-bis-β-D-maltopyranoside (LMNG) and n-decyl-β-D-maltoside (DM) are preferred for both purification and structural studies of MPs (Fig. 1a) (Stetsenko and Guskov, 2017). However, although shorter chain, *i.e.*, C_7–C_{10}, non-ionic detergents, *e.g.*,

n-octyl-β-D-glucoside (OG), have been shown to affect activity of certain classes of MPs (Seddon et al., 2004), they can facilitate obtainment of crystals with high diffraction properties (Parker and Newstead, 2012).

While several non-detergent systems for extraction or stabilization of MPs have been developed, *e.g.*, amphipols (Popot, 2010), nanodiscs (Denisov and Sligar, 2016), peptidiscs (Carlson et al., 2018) or styrene maleic acid co-polymer lipid particles (SMALPs) (Stroud et al., 2018), novel surfactants, including detergents and amphiphiles, are regularly reported (Guillet et al., 2019; Chae et al., 2010; Breibeck and Rompel, 2019). Many of these new generation compounds are DDM analogues, building on its outstanding track record within MP research (Chae et al., 2010; Breibeck and Rompel, 2019; Hong et al., 2010). Recently, the novel DDM derivative was synthetized, 4-trans-(4-trans-propylcyclohexyl)-cyclohexyl α-maltose (t-PCCαM; Fig. 1b), in which the hydrophobic tail compared to the parental linear alkyl chain is bearing two cyclohexyl rings, rendering the molecule overall more rigid (Hovers et al., 2011). Notably, t-PCCαM displayed promising properties in recovering chloroplast ATP synthase from spinach leaves (Hahn et al., 2018), bovine mitochondrial super-complexes (Sousa et al., 2016) or human neutral and basic amino acid transport complex (b[0,+]AT1-rBAT) (Wu et al., 2020), and, as a secondary detergent, maintained stability and permitted crystallization of bacterial cytochrome *b*6f (Hovers et al., 2011) or RC-LH1-PufX (Barret et al., 2013a) complexes. Here we report a comparative analysis of t-PCCαM to isolate a diverse set of MPs from two of the most commonly used heterologous expression platforms, *i.e.*, bacterium *Escherichia coli* and yeast *Saccharomyces cerevisiae*. We have evaluated the performance of t-PCCαM covering multiple aspects of MP studies, including solubilization, affinity purification, structural preservation and activity. Strikingly, t-PCCαM displays favorable behavior for all the assessed MPs, most importantly a uniform distribution of discrete particles in negative staining EM, prerequisite for successful cryo-EM-based structural determination.

2. Results and discussion

2.1. Micellization of t-PCCαM

As reported previously, the CMC value of t-PCCαM is ~5 times lower than that of DDM and both detergents exhibit nearly identical micellar masses, *i.e.*, ~60 kDa (Table 1) (Hovers et al., 2011), although higher M_w (*i.e.*, ~90 kDa) has also been reported for t-PCCαM micelles (Barret et al., 2013a). It cannot be excluded that such discrepancy may be introduced by, *e.g.*, experimental conditions (Fuguet et al., 2005) and has also been observed for DDM (*i.e.*, ~70 kDa) (Strop and Brunger, 2005; Slotboom et al., 2008). Reported aggregation numbers for t-PCCαM and DDM are rather similar (average N_{agg} ~164.5 and ~127.5, respectively) (Barret et al., 2013b). Here, by using dynamic light scattering (DLS), we investigated the properties of self-assembly of both detergents in the applied buffer conditions. From the obtained volume-weighted particle size distributions, we determined the average hydrodynamic radius of 42 and 41 Å for t-PCCαM and DDM, respectively (Table 1), indicating that

Fig. 1. Detergents used for characterization of membrane proteins (MPs).
(a) Cumulative usage of the top four primary surfactants for purification and structure determination of MPs for the period 2015–2019. The evaluation is based on information deposited in the RCSB PDB database (http://www.rcsb.org/) (Berman et al., 2000) extracted by Anatrace (https://www.anatrace.com/). DDM: n-dodecyl-β-D-maltoside; LMNG: 2,2-didecylpropane-1,3-bis-β-D-maltopyranoside; DM: n-decyl-β-D-maltoside. **(b)** Chemical structure of the most commonly employed maltoside detergent in studies of MPs, *i.e.*, DDM, and its novel derivative, *i.e.*, 4-trans-(4-trans-propylcyclohexyl)-cyclohexyl α-maltose (t-PCCαM), characterized in this work.

Table 1
Physicochemical properties of t-PCCαM. Data for DDM are shown for comparison. CMC: critical micelle concentration.

Parameter	t-PCCαM	DDM
Molecular weight, g/mol	548.7[a]	510.6[a]
CMC (room temp), mM	0.036[a]	0.170[a]
CMC (50 °C), mM	0.027[a]	ND
Micellar mass, kDa	62.7 ± 3.5[a]	66.0[a]
Micellar radius, Å	42 ± 0.1[b]	41 ± 1.0[b]

[a] As reported by Hovers et al. (2011)
[b] Results obtained from dynamic light scattering (DLS) measurements. Data represent averages of 30 independent experiments ± SEM. The percent of polydispersity obtained for the samples was 11.4 and 6.03 for DDM and t-PCCαM, respectively.

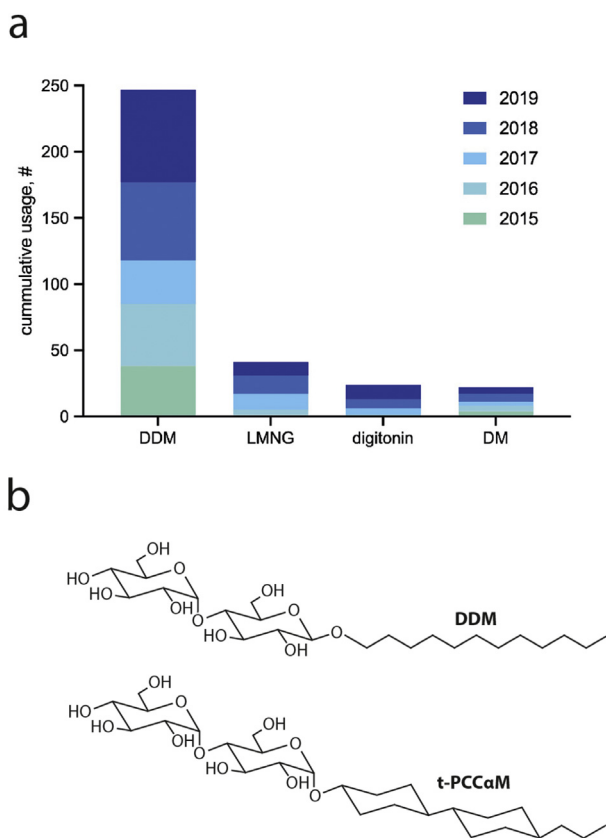t-PCCαM and DDM micelles possess similar molecular weight and diameter.

2.2. Selection of target MPs

To characterize the performance of t-PCCαM, we selected three MPs belonging to different families, originating from diverse species and overproduced in the two separate heterologous platforms (Table 2, Fig. S1). The first tested MP, human aquaporin 10 (hAQP10), is a member of the aquaglyceroporin subfamily (Gotfryd et al., 2018a). This protein is a glycerol facilitator expressed in the small intestine and adipose tissue, and it contributes to energy homeostasis. hAQP10 was overproduced in the yeast *S. cerevisiae* in a N- and C-terminally truncated form with a C-terminal His$_8$-tag fusion (Fig. S1a), in agreement with the structurally determined form (Gotfryd et al., 2018a). The second target, AfCopA from *Archaeoglobus fulgidus*, is a prokaryotic P-type ATPase, permitting efflux of cytoplasmic Cu$^+$ (Padilla-Benavides et al., 2013). AfCopA was expressed as an N-terminal His$_6$-tag fusion lacking the so-called heavy metal binding domains (Fig. S1b), using an *E. coli*-based production platform. The third selected MP, BbZIP, is a zinc transporter from *Bordetella bronchiseptica* belonging to Zrt- and Irt-like protein family (ZIP) (Zhang et al., 2017). BbZIP was overproduced employing *E. coli* in its full-length form fused to N-terminal His$_6$-tag (Fig. S1c).

2.3. Solubilization and stabilization of hAQP10 in t-PCCαM

We first examined the properties of t-PCCαM to extract and stabilize hAQP10. Based on our previous findings, the employed yeast expression platform is able to deliver large amounts of hAQP10 and, importantly, the protein can be efficiently solubilized in DDM from crude *S. cerevisiae* membranes (Bjorskov et al., 2017a). We solubilized identical amounts of the crude yeast membranes overexpressing hAQP10 in either DDM or t-PCCαM (final concentration of 2% w/v). Subsequently, solubilized material was subjected to immobilized-metal affinity chromatography (IMAC) and eluted with an imidazole gradient (Fig. 2a and S2a). The obtained IMAC elution profile for hAQP10 extracted with t-PCCαM (Fig. 2a, red) shares high similarity with the one observed for DM (Fig. S2b), the detergent that was previously used for solubilization and affinity purification of the hAQP10 sample used for crystallization (Gotfryd et al., 2018b). For both t-PCCαM and DM, the main hAQP10 peak (2) eluted at 500 mM imidazole, while a preceding minor peak (1), eluted during the linear part of the gradient (50–500 mM imidazole), corresponded to only ~5% of the total protein yield (Fig. 2a and S2a, red). Conversely, DDM-solubilized hAQP10 yielded mainly peak (1) with the remaining ~5% (peak 2) eluted at 500 mM imidazole (Fig. 2a and S2a, blue). Despite differences in the distribution of peaks in the respective IMAC profiles, we did not observe any major changes in purity of hAQP10 purified in t-PCCαM and DDM (Fig. S3a). Overall, both tested detergents display similar extraction properties as reflected by the total protein yields obtained in each preparation, ranging from 3.3 to 3.5 mg per 1-L culture for t-PCCαM and DDM, respectively.

Next, fractions originating from the two peaks of each IMAC-based purification were pooled and concentrated separately. Subsequently, the samples were subjected to size-exclusion chromatography (SEC) to evaluate the homogeneity. The protein derived from the main IMAC peak (1) of DDM-solubilized hAQP10 showed high degree of aggregation as it eluted mainly in the void volume (~8 mL), with only a marginal amount eluting at the typical retention volume observed for this target, *i.e.*, ~11 mL (Fig. 2b, blue). Conversely, the remaining IMAC peak (2) of DDM-purified hAQP10 displayed high grade of homogeneity, eluting as a symmetric peak at ~11 mL (Fig. 2c, blue), similarly to what is typically observed for SEC profile of hAQP10 obtained in n-nonyl-β-D-glucoside (NG, Fig. S2c) or OG (Bjorskov et al., 2017a). In case of hAQP10 purified in t-PCCαM, the SEC profile obtained for IMAC peak (1) revealed the existence of two protein populations reflected by the two monodispersed peaks (Fig. 2b, red). However, none of the two peaks indicated protein aggregation, displaying elution following the column void volume. Hence, they likely represent two oligomeric states of hAQP10 present in the sample, the latter corresponding to the hAQP10 monomer. SEC analysis of the main IMAC peak (2) of hAQP10 purified in t-PCCαM resulted in a monodisperse profile preceded by a minor shoulder, indicating a high degree of homogeneity of the sample in the oligomeric state (Fig. 2c, red). Collectively, although both tested detergents were demonstrated to extract hAQP10 from the yeast membranes with similar efficacy, t-PCCαM was able to provide significantly larger amount of protein stabilized in the native oligomeric state.

DLS measurements on hAQP10 showed that the autocorrelation curve for the t-PCCαM sample is slightly shifted to the left when compared to the DDM sample (Fig. 3a). This indicates the presence of particles with smaller hydrodynamic radius in t-PCCαM as compared to DDM in solution and also corroborates that less aggregates in suspension are contributing to the scattering signal. Subsequently, by applying nanoscale differential scanning fluorimetry (nanoDSF), we assessed thermal stability of the hAQP10 samples purified in both detergents (Fig. 3b). Analysis of the estimated melting temperatures (T$_m$s) revealed that hAQP10 solubilized and IMAC-purified in t-PCCαM displayed increased stability as compared to the DDM-derived sample, concerning the peak (1) fractions. The peak (2) samples appear more stable in both detergents as reflected by the higher onset temperature for denaturation (T$_{onset}$, Table S1). In conclusion, the sample solubilized in t-PCCαM exhibited the highest T$_m$ and hence stability (Fig. 3b).

To evaluate whether t-PCCαM also preserves protein activity, we performed functional characterization of the SEC-purified samples originating from IMAC peaks (2) for both detergents. Here we reconstituted the samples into lipid vesicles and assessed water flux in the resulting proteoliposomes (Kitchen et al., 2020). As investigated by the stopped-flow kinetic assay where water permeability is estimated from obtained fluorescence traces (Fig. 4a), hAQP10 exhibited activity in both tested detergents. Sample derived from t-PCCαM-purified hAQP10 showed moderately higher water flux rate (k) of 14.2 s^{-1} (Fig. 4a, red) as compared with DDM-solubilized protein (flux rate of 12.6 s^{-1}; Fig. 4a, blue). Furthermore, t-PCCαM-purified hAQP10 displayed marginally lower water conductance as compared with DM-derived sample (*i.e.*, 20.0 s^{-1}, Fig. S2d, red *vs* orange). However, it has to be stressed that the

Table 2
Membrane proteins (MPs) and quality control assays used for characterization of t-PCCαM. SEC: size-exclusion chromatography; EM: electron microscopy; nanoDSF: nanoscale differential scanning fluorimetry; ZIP: Zrt- and Irt-like protein family.

Target (UniProt ID)[a]	Organism	MP family	Primary function	Expression host	Quality control assessment
hAQP10 (Q96PS8)	*Homo sapiens*	Aquaporin	Glycerol facilitator	*Saccharomyces cerevisiae*	SEC, negative stain EM, nanoDSF, activity assay
AfCopA (O29777)	*Archaeoglobus fulgidus*	P$_{1B-1}$-type ATPase	Cu$^+$ transporter	*Escherichia coli*	SEC, negative stain EM, activity assay
BbZIP (A0A0H3LM39)	*Bordetella bronchiseptica*	ZIP	Zn^{2+} transporter	*Escherichia coli*	SEC

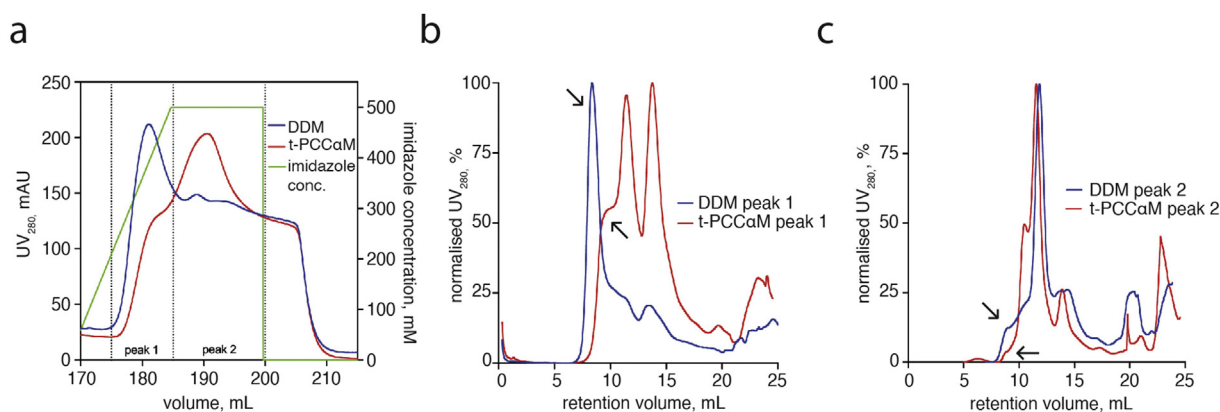[a] UniProt database is accessible at: https://www.uniprot.org/(UniProt, 2019)

Fig. 2. Purification of human aquaporin 10 in DDM or t-PCCαM. (a) Immobilized-metal affinity chromatography (IMAC)-based purification of hAQP10 expressed in a 2-L scale in shaker flasks and solubilized from the same amount of crude *Saccharomyces cerevisiae* membranes in 2% w/v of DDM (blue) or t-PCCαM (red). IMAC profiles indicate the UV$_{280}$ signal using an imidazole gradient of 50–500 mM (green). **(b)** and **(c)** Normalized size-exclusion chromatography (SEC) profiles originating from pooled IMAC fractions corresponding to peak (1) **(b)** eluted with 50–500 mM imidazole gradient or in peak (2) **(c)** eluted in the 500 mM imidazole and produced in DDM (blue) or t-PCCαM (red). SEC was performed using a Superdex 200 Increase 10/300 GL column by monitoring the A$_{280}$ signal. Arrows indicate the position of fractions eluted at the void volume (~8 mL).
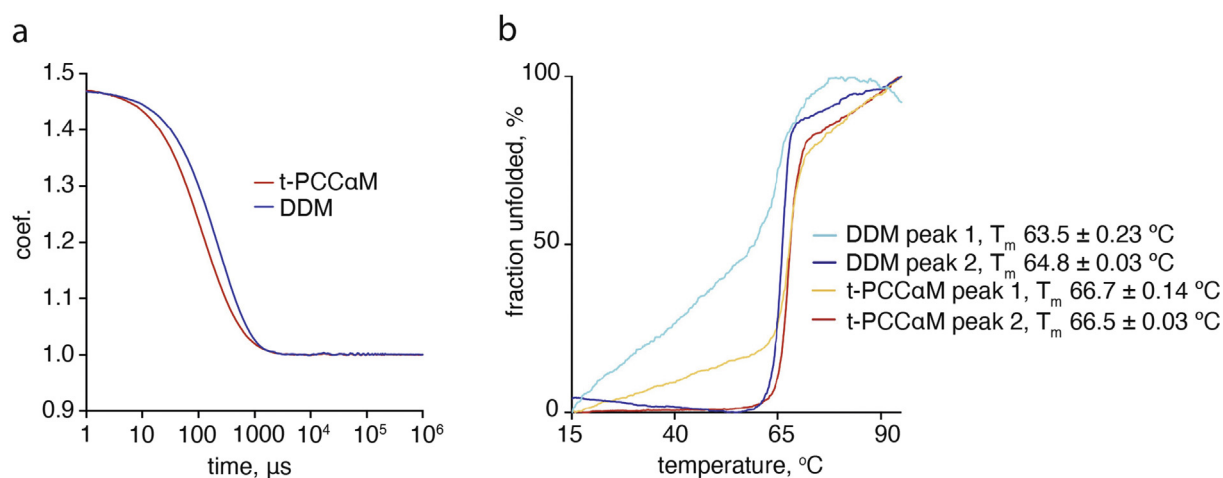

Fig. 3. Physicochemical properties of human aquaporin 10 purified in DDM or t-PCCαM. (a) Dynamic light scattering autocorrelation functions of immobilized-metal affinity chromatography (IMAC)-purified hAQP10 in t-PCCαM (red) or DDM (blue) originating from peak (1) obtained in runs shown in Fig. 2a. The curves represent an average from 30 measurements. The mean hydrodynamic radius value extracted from the curves for the range 0.1–10 nm is ~50 *vs* ~59 nm for t-PCCαM and DDM, respectively. **(b)** Thermal denaturation curves originating from pooled immobilized-metal affinity chromatography fractions of IMAC-purified hAQP10 in DDM (peak (1) in cyan and peak (2) in dark blue), and in t-PCCαM (peak (1) in orange and peak (2) in red), see Fig. 2a. The nanoscale differential scanning fluorimetry curves are based on two replicates. Melting temperatures (T$_m$, °C) for hAQP10 sample purified in DDM or t-PCCαM are also indicated. T$_m$ was obtained by curve fitting of nanoscale differential scanning fluorimetry curves (F$_{350}$/F$_{330}$ ratio) for the respective IMAC peaks, see Fig. 2a.

applied reconstitution procedure was optimized mainly for DM detergent, which in turn can affect the overall measured activity of hAQP10 samples prepared in other surfactants.

Finally, to further asses sample quality, we evaluated SEC-grade hAQP10 originating from IMAC peaks (2) for both detergents by employing negative staining EM and focusing on particle distribution and homogeneity. Negative stain micrographs of hAQP10 purified in t-PCCαM showed monodisperse particles with only few examples of heavily stained, variably sized particles that could indicate aggregates or contaminants (Fig. 4b). In contrast, negatively-stained DDM-solubilized sample revealed a lower degree of monodispersity with large number of particles that varied significantly in size and accumulated stain (Fig. 4c), indicative of decreased level of homogeneity and purity. All-in-all, it can be concluded that t-PCCαM appears compatible with isolation, purification, stabilization and biophysical applications of yeast-derived human aquaporin member, matching the available state-of-the-art detergents for this protein family.

2.4. Solubilizing and stabilizing properties of t-PCCαM on AfCopA

We then evaluated the effects of t-PCCαM on the bacterial Cu$^+$-ATPase from *A. fulgidus* (AfCopA) that was overexpressed and purified from an *E. coli*-based platform according to previously established procedures (Gourdon et al., 2011a). Here we performed identical purification principles as for hAQP10, including solubilization from isolated crude membranes, IMAC and SEC. Following solubilization of the same amount of bacterial membrane material (with the final detergent concentration of 1% w/v) and affinity purification, the resulting IMAC elution profiles and purities of AfCopA obtained in t-PCCαM and DDM were almost identical (Fig. 5a, S3b and S4a). Importantly, the total protein yield for t-PCCαM-purified AfCopA was marginally higher as compared to the DDM-solubilized sample, with 5.6 *vs* 4.7 mg of protein per 1-L of cell culture, respectively. For comparison, typical purification of AfCopA in dodecyl octaethylene glycol ether (C$_{12}$E$_8$) upon solubilization in DDM typically yields 7–8 mg of protein per 1-L of cell culture (Fig. S4b). Obtained SEC profiles of AfCopA in t-PCCαM and DDM were
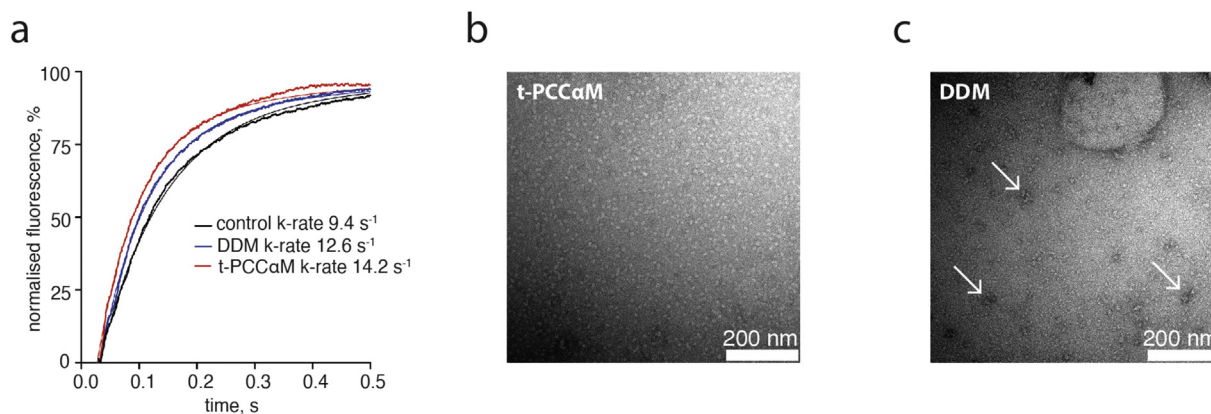
Fig. 4. Characterization of human aquaporin 10 purified in DDM or t-PCCαM. (a) Activity of size-exclusion chromatography (SEC)-purified hAQP10 samples (originating from immobilized-metal affinity chromatography (IMAC) peak (2) obtained in runs shown in Fig. 2c) and reconstituted into proteoliposomes. Normalized fluorescence traces from a water flux assay are presented for the proteoliposomes containing hAQP10 samples purified in DDM (blue) and t-PCCαM (red). Signal derived from control (*i.e.*, empty) liposomes is shown in black. The data were obtained from 3 separate reconstitutions, where each curve was averaged from 10 stopped-flow traces and fitted to a double exponential function (solid curves with the corresponding colors). The calculated water flux rate constants (k, s^{-1}) are indicated in the figure legend. **(b)** and **(c)** Electron microscopy (EM) negative staining of hAQP10 samples also used in panel (a) in the presence of t-PCCαM **(b)** and DDM **(c)**, respectively. Scale bars: 200 nm. Arrows indicate particles with accumulated stain indicative of sample aggregation or contamination.

again comparable, with the protein peaks eluting at similar retention volumes (Fig. 5b). However, the sample purified in t-PCCαM showed a slightly lower void-to-peak ratio and the resulting protein peak was more monodisperse as compared to the DDM-solubilized sample. SDS-PAGE

analysis of the main peak fractions did not reveal any differences between the two tested detergents (Fig. S3b). In conclusion, the SEC profile of t-PCCαM-purified AfCopA resembles more the one typically observed during the purification in $C_{12}E_8$ (Fig. S4c).
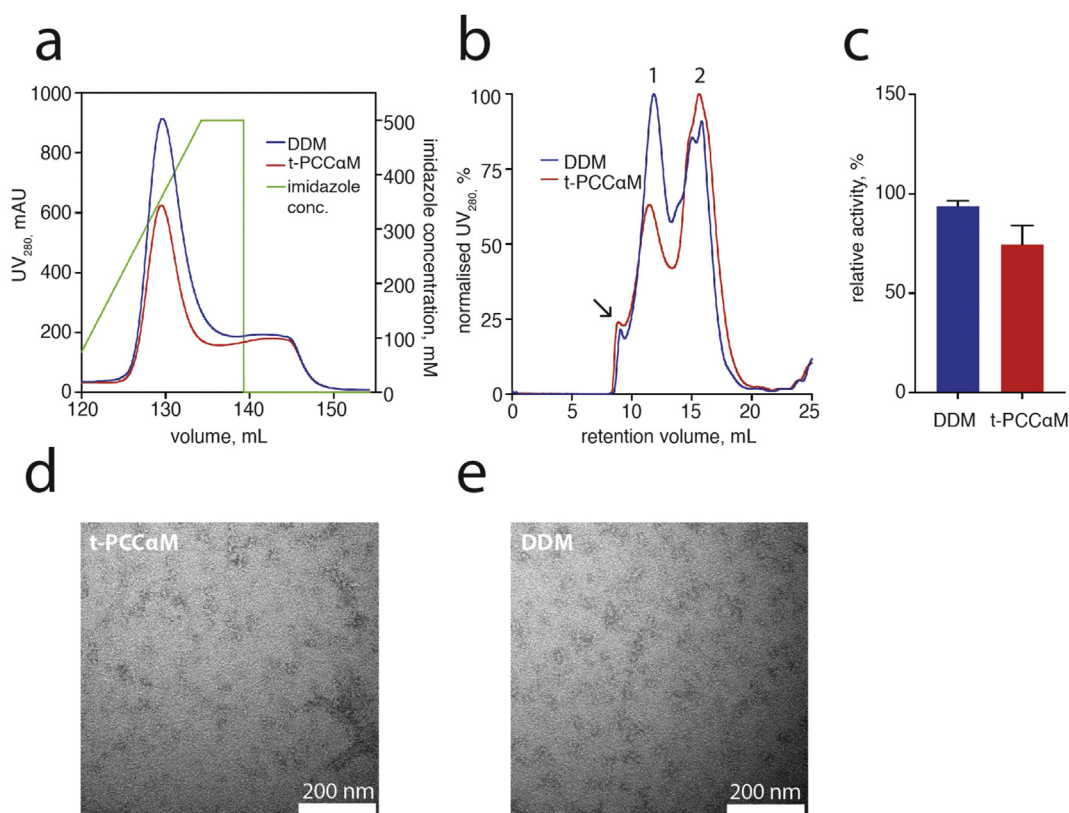

Fig. 5. Purification and characterization of the P-type ATPase AfCopA in DDM or t-PCCαM. (a) Immobilized-metal affinity chromatography (IMAC)-based purification of AfCopA expressed in a 2-L scale in shaker flasks and solubilized from the same amount of crude *Escherichia coli* membranes in 1% w/v of DDM (blue) or t-PCCαM (red). IMAC profiles indicate the UV_{280} signal using an elution with 50–500 mM imidazole gradient (green). **(b)** Normalized size-exclusion chromatography (SEC) profiles originating from pooled IMAC fractions produced in DDM (blue) or t-PCCαM (red). SEC was performed using a Superose 6 10/300 GL column by monitoring the A_{280} signal. Arrow indicates the position of shoulders eluted at the void volume (~8 mL). **(c)** Activity (%) of SEC-purified AfCopA samples (originating from SEC peak (2) using the so-called Baginski assay. Data were normalized relative to the activity obtained in dodecyl octaethylene glycol ether ($C_{12}E_8$, Fig. S4d) and represent averages of three independent experiments ± SEM. **(d)** and **(e)** Electron microscopy (EM) negative staining of SEC-purified AfCopA samples. Negative-stain EM micrographs of AfCopA purified in t-PCCαM **(d)** and DDM **(e)** are shown. Scale bars: 200 nm.

To assess activity of SEC-purified (peak (2)) AfCopA obtained in t-PCCαM and DDM, we conducted the so-called Baginski assay, a well-established *in vitro* ATPase functional characterization method based on the colorimetric detection of the free inorganic phosphate generated from hydrolysis of ATP (Baginski et al., 1967). DDM-derived AfCopA exhibited marginally higher activity compared to t-PCCαM (Fig. 5c), but moderately lower functionality compared to the sample obtained in $C_{12}E_8$ (Fig. S4d), the most commonly used surfactant for purification of CopA or other P-type ATPases (Sorensen et al., 2004; Toyoshima et al., 2000).

To evaluate the quality of t-PCCαM-solubilized SEC-purified AfCopA sample further, we also performed negative staining EM. Analysis of the obtained negative stain micrographs revealed that AfCopA purified in both t-PCCαM and DDM exhibited identical particle distribution and quality (Fig. 5d and e, respectively), with areas indicating patches of aggregation. Noteworthy, it has previously been shown that AfCopA exhibits fibril-like particle formation when performing EM (Allen et al., 2011). Thus, it can be speculated that the possible aggregation pattern observed here resembles rather protein fibrils, since the particles aggregate in a more linear shape and do not form large clusters. Taken together, these results indicate that even though minor differences in protein yield and activity are observed between the two compared detergents, t-PCCαM is fully capable of delivering stable and active AfCopA.

2.5. Effects of t-PCCαM on solubilization and stabilization of BbZIP

To further assess the effects of t-PCCαM, we turned to the only successfully produced and structurally characterized member of the ZIP family, a zinc transporter from *B. bronchiseptica* (BbZIP) (Zhang et al., 2017). This MP class has previously been categorized as difficult to express and purify in a stable form (Lin et al., 2010). Similar to AfCopA, BbZIP was also expressed using *E. coli* as the production host; however, in the case of this target, the obtained protein yields are typically notably lower. To investigate the effects of t-PCCαM on BbZIP, we first performed solubilization with the final detergent concentration of 2% w/v using equal amount of isolated bacterial membranes. Subsequently, IMAC purification was conducted and resulted with nearly identical elution profiles for both t-PCCαM and DDM (Fig. 6a and S5). Moreover, the yields of purified BbZIP protein were very similar (*i.e.*, ~3 mg per 1-L of cell

culture) together with the overall purity of the samples, including the fraction retained as a native dimer (Fig. S3c), indicative of the mild properties of t-PCCαM detergent.

To determine quality and homogeneity of the t-PCCαM-solubilized sample, we performed SEC-based analysis. Strikingly, whereas approximately half of the DDM-purified BbZIP eluted as void peak, reflecting large protein aggregation (Fig. 6b, blue), the vast majority of the sample produced in t-PCCαM remained stable (Fig. 6b, red) and eluted at the retention volume typically observed for DDM-solubilized BbZIP (*i.e.*, ~11.5 mL). Moreover, assessment of the SEC-grade samples revealed slightly higher purity of t-PCCαM-solubilized BbZIP as compared with DDM-derived protein (Fig. S3c).

Identically to hAQP10 and AfCopA, we also attempted to evaluate SEC-purified t-PCCαM-solubilized BbZIP employing negative staining EM. Unfortunately, both t-PCCαM- and DDM-solubilized samples exhibited severe aggregation during staining and no conclusive results were obtained (data not shown). This highlights the overall difficulty in handling ZIP family members due to their instability and hence more optimization of the BbZIP isolation procedures should be considered before this target can be applied for subsequent downstream biophysical analysis.

3. Conclusions

Extraction of MPs from the native lipid environment with concomitant maintenance of their native state and activity is one of the most challenging tasks within the structural biology field. We here performed a systematic characterization of the DDM derivative, t-PCCαM, and demonstrated that it represents a powerful tool for solubilization and stabilization of three selected and separate types of MPs produced in two expression host systems. Physicochemically, t-PCCαM forms micelles with a less flexible hydrophobic core and more compact protein-detergent complexes than DDM, desirable features in structural studies of MPs (Prive, 2007; Breibeck and Rompel, 2019; Mio and Sato, 2018; Mineev and Nadezhdin, 2017). This tighter assembly of empty micelles by t-PCCαM may indeed be superior to DDM in respect to easiness of their removal, an important parameter as elevated concentration of detergents can have detrimental effects on both crystallization and cryo-EM efforts. Importantly, smaller protein-detergent complexes are likely beneficial in
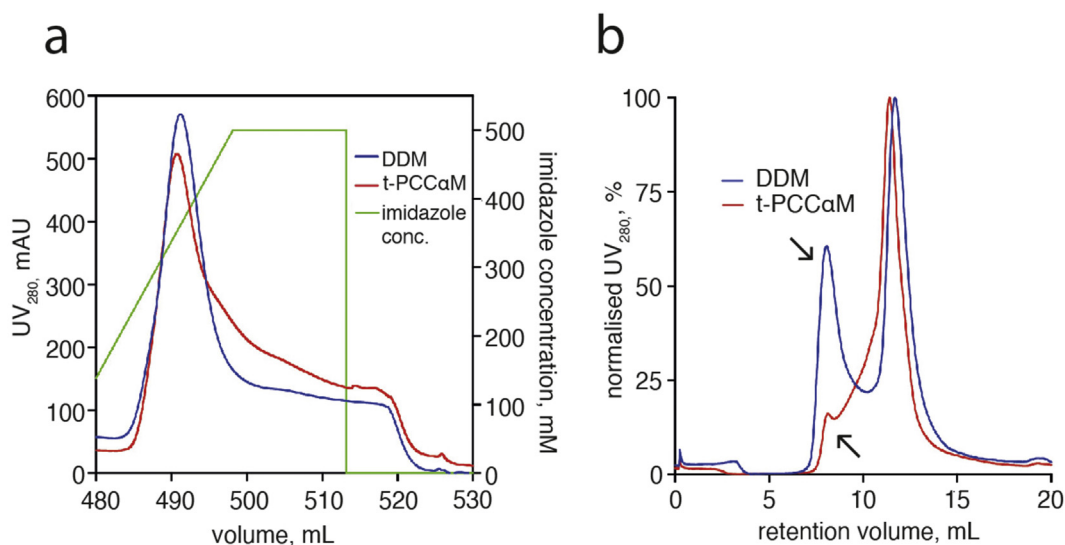

Fig. 6. Purification and characterization of BbZIP protein in DDM or t-PCCαM. (a) Immobilized-metal affinity chromatography (IMAC)-based purification of BbZIP expressed in a 2-L scale in shaker flasks and solubilized from the same amount of crude *Escherichia coli* membranes in 2% w/v of DDM (blue) or t-PCCαM (red). IMAC profiles indicate the UV_{280} signal using an elution with 50–500 mM imidazole gradient (green). **(b)** Normalized size-exclusion chromatography (SEC) profiles originating from pooled IMAC fractions produced in DDM (blue) or t-PCCαM (red). SEC was performed using a Superdex 200 Increase 10/300 GL by monitoring the A_{280} signal. Arrows indicate the position of fractions eluted at the void volume (~8 mL).

formation of crystal contacts, providing well-defined NMR spectra or in establishing more uniform cryo-EM specimens.

Overall, t-PCCαM exhibited similar potency as compared to DDM in extracting the tested MPs. However, the stabilizing properties of t-PCCαM were superior to DDM. Strikingly, t-PCCαM improved the thermostability of hAQP10, a target that displays already high initial stability in different detergents. Here t-PCCαM allowed for production of more uniformed IMAC-grade sample exhibiting high monodispersity (as assessed by SEC and negative staining EM) and activity. Similar results were obtained for AfCopA, where the stabilizing effect of t-PCCαM was marginally better than for DDM. In case of the least stable target, *i.e.*, BbZIP, t-PCCαM provided significantly enriched population of monodisperse SEC-grade protein than DDM. However, this improvement of the stability was insufficient to perform negative staining EM-based analysis on BbZIP, indicating that further optimization of the isolation procedure is necessary for this target.

All-in-all, based on these findings we conclude that t-PCCαM is a highly suitable and competitive surfactant to be included in both start-up solubilization screens and to be considered as a secondary detergent in final steps of MP sample preparation. Based on the studies of members of three separate target families of MPs, we believe that this detergent can be successfully applied to a broader portfolio of challenging MPs for downstream biophysical applications.

4. Materials and methods

4.1. Production of hAQP10

Human AQP10 (hAQP10) was produced essentially as previously described (Gotfryd et al., 2018b; Bjorkskov et al., 2017b). Briefly, the protein was overexpressed in the *S. cerevisiae* PAP1500 strain (α ura3-52 trp1: GAL10-GAL4 lys2-801 leu2Δ1 his3Δ200 pep4:HIS3 prb1Δ1.6R can1 GAL) transformed with the pPAP2259 vector (Pedersen et al., 1996) encoding an N- (Δ1-10) and C-terminally (Δ277-301) truncated hAQP10 fused to a C-terminal octa-histidine (His$_8$) stretch. Yeast was grown in shaker flasks in minimal medium supplemented with 0.1 mg/mL ampicillin and V200. Cells were propagated to OD$_{600}$ = 1.0–1.5 at 30 °C and 100 r.p.m. Protein expression was induced with a final concentration of 2% w/v galactose at 15 °C for 24 h prior to harvesting. Cells were resuspended in a lysis buffer (25 mM Tris-HCl pH 7.5, 500 mM NaCl, 20% v/v glycerol and 5 mM β-mercaptoethanol, BME) supplemented with 1 mM phenylmethylsulfonyl fluoride (PMSF) and 1 μg/mL of leupeptine, pepstatin and chymostatin (LPC; Sigma Aldrich, USA). Following cell homogenization using a bead beating system (BioSpec, USA), cell debris-free material was ultracentrifuged at 190,000×*g*, 4 °C for 3 h using a Beckman Ti-45 rotor (Beckman, USA). Isolated crude membranes were then resuspended in a solubilization buffer (20 mM Tris-HCl pH 7.5, 200 mM NaCl, 20% v/v glycerol and 5 mM BME) supplemented with 1 mM PMSF and 1 μg/mL of LPC, followed by solubilization in 2% w/v n-dodecyl-β-D-maltoside (DDM; Anatrace, USA) or t-PCCαM (Glycon Biochemicals, Germany) (Hovers et al., 2011) for 4 h at 4 °C. Solubilized material was subsequently diluted twice to reduce the final detergent concentration and bound to a 5-mL nickel-charged affinity HisTrap HP column (Cytiva, Denmark). Following washes, the protein was eluted in immobilized-metal affinity chromatography (IMAC) buffer (20 mM Tris-HCl pH 7.5, 200 mM NaCl, 20% v/v glycerol, 5 mM BME and 500 mM imidazole) supplemented with 0.03% w/v DDM or t-PCCαM. Purified hAQP10 was subsequently concentrated using Vivaspin concentrators (MWCO 100 kDa; Sartorius, Germany) and size-exclusion chromatography (SEC) was performed using a Superdex 200 Increase 10/300 GL column (Cytiva) equilibrated with a SEC buffer (20 mM Tris-HCl pH 8.0, 100 mM NaCl, 10% v/v glycerol and 2 mM BME) containing 0.03% w/v DDM or t-PCCαM.

4.2. Dynamic light scattering (DLS) measurements

DLS measurements were performed using a DynaPro Nanostar device and the data were processed with Dynamics v.7 software (both from Wyatt Technology Corporation, USA). Samples were centrifuged at 10,062×*g* for 10 min prior to measurements performed at 25 °C using 4-μL plastic cuvettes (Wyatt Technology Corporation). The acquisition time was 5 s with and a total of 30 acquisitions were averaged.

4.3. Nanoscale differential scanning fluorimetry (nanoDSF) measurements

Each sample was used to fill two standard grade nanoDSF capillaries (Nanotemper, Germany) and loaded into a Prometheus NT.48 device (Nanotemper) controlled by the PR.ThermControl v.2.1.2 software. Excitation power was pre-adjusted to get fluorescence readings above 2000 RFU for F330 and F350, and samples were heated from 15 to 95 °C with a slope of 1 °C/min. An XLSX file containing the processed nanoDSF data was exported from PR.ThermControl and used for further analysis to extract the melting (T$_m$) and onset denaturation (T$_{onset}$) temperatures (Kotov et al., 2019). Normalization of curves to calculate the fraction of unfolded protein was performed using the MoltenProt software (Kotov et al., 2021).

4.4. Reconstitution of hAQP10 into liposomes and water flux activity assay

Reconstitution of hAQP10 was performed as previously reported (Kitchen et al., 2020). Empty liposomes were prepared using *Escherichia coli* polar lipid extract (Avanti Polar Lipids, USA) rehydrated to a lipid concentration of 20 mg/mL in a reconstitution buffer (20 mM HEPES-NaOH pH 8 and 200 mM NaCl) supplemented with 10 mM 5(6)-carboxyfluorescein (Sigma Aldrich). Following sonication steps, the lipid solution was flash-frozen and passed through a 200-nm polycarbonate filter mounted in an extruder (Avanti Polar Lipids). The lipids were then diluted to 4 mg/mL in the reconstitution buffer containing 25% v/v glycerol, 0.4% w/v n-nonyl-β-D-glucoside (NG; Anatrace) and 0.02% Triton X-100 (Sigma Aldrich). Subsequently, SEC-purified hAQP10 was added to the lipid solution to a lipid-to-protein ratio of 100 (w/w) and the sample was dialyzed O/N at 4 °C against the reconstitution buffer. The samples were centrifuged at 57,000×*g* for 1.5 h and the resulting pellets were dissolved in the reconstitution buffer. All reconstitutions were performed in triplicates. The stopped-flow measurements of water flux were performed using an SX-20 Stopped-Flow Spectrometer (Applied Photophysics, UK), permitting rapid mixing of the proteoliposomes with the reaction buffer (20 mM HEPES-NaOH pH 8 and 500 mM NaCl). Data were collected at the excitation wavelength of 495 nm for 2 s at room temperature. Empty liposomes served as a negative control to estimate background water flux rates. The data were analyzed and plotted using GraphPad Prism v.8 software (GraphPad Software, USA). Each sample was measured ten times, then averaged, normalized and fitted using a double exponential model. The smaller k rate is unaffected by changes in the reconstitution efficiency, and hence the larger k rate represents the overall kinetics of water flux mediated by the reconstituted hAQP10.

4.5. Production of AfCopA

CopA from *Archaeoglobus fulgidus* (AfCopA) was expressed in *E. coli* as a variant lacking its N- and C-terminal heavy metal binding domains (AfCopAdNC), essentially as previously described for CopA from *Legionella pneumophila* (Gourdon et al., 2011b). Briefly, a pET22b(+) vector encoding the AfCopA gene N-terminally fused to a His$_6$ stretch was transformed into the *E. coli* C43 strain. Cell cultures were performed in LB medium supplemented with 0.1 mg/mL ampicillin in shaker flasks. Cells were grown to OD$_{600}$ = 0.6–0.8 at 37° and 120 r.p.m. before protein

expression was induced with 1 mM IPTG. Induction was performed for 16 h at 20 °C and 120 r.p.m., before the cells were harvested, resuspended in a lysis buffer (20 mM Tris-HCl pH 7.6, 200 mM KCl and 20% v/v glycerol) in a volume of 5 mL per 1 g and stored at −80 °C. Thawed cell material was supplemented with 5 mM BME, 2 μg/mL DNase, 1 mM MgCl$_2$ and 1 μg/mL LPC. The cells were broken by passing the suspension through a cell disruptor twice at 25 kpsi pressure (Constant Systems Limited, UK) and 1 mM PMSF was added to the lysate immediately after homogenization. Subsequently, cell debris was removed and the lysate was ultracentrifuged at 190,000×*g*, 4 °C for 3 h. Isolated crude membranes were resuspended in a solubilization buffer (20 mM Tris-HCl pH 7.6, 200 mM KCl, 20% v/v glycerol, 5 mM BME and 1 mM MgCl$_2$) supplemented with 1 mM PMSF and 1 μg/mL LPC at 0.1 g membranes per 1 mL buffer and stored at −80 °C. Following determination of protein concentration using Bradford assay (Thermo Fisher Scientific, USA), an even amount of membranes was solubilized at a total protein concentration of 3 mg/mL in 1% DDM (Anatrace) or t-PCCαM (Glycon Biochemicals) for 2 h at 4 °C. Insolubilized material was removed by ultracentrifugation (190,000×*g*, 4 °C, 1 h), and the supernatant was supplemented with 30 mM imidazole and 500 mM KCl before loading on a 5-mL HisTrap HP column (Cytiva). The column was washed with 50 mL of an IMAC buffer (20 mM Tris-HCl pH 7.6, 200 mM KCl, 20% v/v glycerol, 5 mM BME and 1 mM MgCl$_2$) containing either 0.03% w/v DDM (Anatrace), 0.03% w/v t-PCCαM (Glycon Biochemicals) or 0.015% w/v dodecyl octaethylene glycol ether (C$_{12}$E$_8$; Nikko Chemicals, Japan) and supplemented with 50 mM imidazole. Bound AfCopA was then eluted in the corresponding IMAC buffers supplemented with 500 mM imidazole. IMAC-purified protein was concentrated to 20 mg/mL using Vivaspin concentrators (MWCO 50 kDa; Sartorius) and the samples were injected on a Superose 6 10/300 GL column (Cytiva) equilibrated in a SEC buffer (20 mM Tris-HCl pH 7.6, 80 mM KCl, 20% v/v glycerol, 5 mM BME and 3 mM MgCl$_2$) containing either 0.03% w/v DDM (Anatrace), 0.03% w/v t-PCCαM (Glycon Biochemicals) or 0.015% w/v C$_{12}$E$_8$ (Nikko Chemicals).

4.6. Negative staining EM

SEC-purified hAQP10 and AfCopA were diluted to 10 μg/mL in the respective SEC buffers. Subsequently, 4 μL of the sample was applied to glow-discharged, 400 mesh carbon-coated grid (Quantifoil Micro Tools GmbH, Germany) and incubated for 1 min. The grids were stained with 4 μL of 2% w/v uranyl acetate and washed with 4 μL of water for 1 min, followed by drainage with a filter paper. Negative stain EM micrographs were taken on a Philips CM100 transmission electron microscope (Philips, UK) operated at 100 kV.

4.7. AfCopA activity assay

The activity of AfCopA was determined using SEC-purified samples concentrated to 10 mg/mL and employing the so-called Baginski assay (Baginski et al., 1967). Briefly, 0.05 mg/mL protein was added to a reaction buffer (40 mM MOPS-KOH pH 6.8, 150 mM NaCl, 5 mM KCl and 5 mM MgCl$_2$) supplemented with 0.2 mg/mL L-α-phosphatidylcholine from soybean, 10 mM cysteine, 5 mM Tris(2-carboxyethyl)phosphine, 20 mM ammonium sulfate, 5 mM sodium nitrate, 0.25 mM sodium molybdate and 0.5 mM ammonium tetrathiomolybdate (all from Sigma Aldrich), and either 0.33 mg/mL of DDM (Anatrace), t-PCCαM (Glycon Biochemicals) or C$_{12}$E$_8$ (Anatrace). Subsequently, 1 mM CuCl$_2$ was added following incubation for 15 min at RT. The assay was performed at 72 °C and the samples were incubated 5 min before the reaction was started by adding 5 mM ATP (Sigma Aldrich). For a total of 40 min, 50 μL of the respective reaction mixtures was transferred to a 96-well microplate at 5–10 min intervals and mixed with an equal volume of ascorbic acid

solution (formed by mixing a solution containing 0.17 M ascorbic acid and 0.1% SDS in 0.5 M HCl with aqueous 28.3 mM ammonium heptamolybdate in a 5:1 ratio, all from Sigma Aldrich). After incubation for 10 min at RT, 75 μL of sodium arsenic solution (consisting of 0.068 M trisodium citrate, 0.154 M sodium metaarsenic and 2% v/v glacial acetic acid, all from Sigma Aldrich) was added to stop color development. After 30-min incubation, the absorbance was measured at 860 nm for the samples prepared in triplicates in three independent experiments.

4.8. Production of BbZIP

BbZIP from *Bordetella bronchiseptica* was expressed in its full-length form as an N-terminal His$_6$ stretch fusion. The resulting construct was cloned into pET15b(+) vector and transformed into the *E. coli* C43 strain. Cells were grown in TB media supplemented with 0.1 mg/mL ampicillin in shaker flasks to OD$_{600}$ = 0.8 at 37 °C and 150 r.p.m. Subsequently, protein expression was induced with 1 mM IPTG for 24 h at 20 °C before the culture was harvested and stored at −80 °C. Cells were resuspended in a lysis buffer (25 mM HEPES-NaOH pH 7.0, 500 mM NaCl and 20% v/v glycerol) supplemented with 1 μg/mL LPC and mechanically disrupted (Constant Systems Limited) before the cell homogenate was supplemented with 1 mM PMSF. Upon removal of the cell debris, crude membranes were isolated by ultracentrifugation at 190,000×*g*, 4 °C for 3 h and resuspended in a solubilization buffer (20 mM HEPES-NaOH pH 7.3, 200 mM NaCl a 20% v/v glycerol) supplemented with 0.1 mM CdCl$_2$, 1 μg/mL LPC and 1 mM PMSF to a protein concentration of 5 mg/mL. An even amount of membranes was solubilized with either 2% w/v DDM (Anatrace) or t-PCCαM (Glycon Biochemicals) for 3 h at 4 °C. Following two-fold dilution of the material in the solubilization buffer to reduce final detergent concentration, the samples were supplemented with 50 mM imidazole and 500 mM NaCl, and loaded onto a 5-mL HisTrap HP column (Cytiva). After column wash with an IMAC buffer (50 mM HEPES-NaOH pH 7.3, 200 mM NaCl, 20% v/v glycerol and 500 mM imidazole) containing either 0.1% w/v DDM (Anatrace) or 0.1% w/v t-PCCαM (Glycon Biochemicals), bound BbZIP was eluted with 50–500 mM imidazole gradient. Subsequently, the purified protein was dialyzed O/N at 4 °C against the corresponding IMAC buffers and concentrated to 8 mg/mL using Vivaspin concentrators (MWCO 10 kDa; Sartorius). Finally, SEC was performed employing a Superdex 200 increase 10/300 column (Cytiva) equilibrated with the SEC buffer (20 mM NaOAc pH 4.5, 200 mM NaCl, 15% v/v glycerol) supplemented with either 0.03% w/v DDM (Anatrace) or 0.03% w/v t-PCCαM (Glycon Biochemicals).

thank the Core Facility for Integrated Microscopy (CFIM; Department of Biomedical Sciences, Copenhagen University) for assistance with negative staining EM and Prof. Michael Davies for providing access to the stopped-flow cytometer. The present work was primarily supported by the Lundbeck Foundation (R133-A12689 & R313-2019-774), the Knut and Alice Wallenberg Foundation (KAW 2015.0131), the Independent Research Fund Denmark (6108–00479 & 9039–00273) and NordForsk (82000). The funders had no role in study design, data collection and analysis, decision to publish or preparation of the manuscript. We acknowledge technical support by the SPC facility at EMBL Hamburg funded through the Hanseatic League of Science Cross Border Research.

Appendix A. Supplementary data

Supplementary data to this article can be found online at https://doi.org/10.1016/j.crstbi.2021.03.002.

References

Allen, G.S., Wu, C.C., Cardozo, T., Stokes, D.L., 2011. The architecture of CopA from Archeaoglobus fulgidus studied by cryo-electron microscopy and computational docking. Structure 19 (9), 1219–1232.

Almen, M.S., Nordstrom, K.J.V., Fredriksson, R., Schioth, H.B., 2009. Mapping the human membrane proteome: a majority of the human membrane proteins can be classified according to function and evolutionary origin. BMC Biol. 7.

Anandan, A., Vrielink, A., 2016. Detergents in membrane protein purification and crystallisation. Adv. Exp. Med. Biol. 922, 13–28.

Baginski, E.S., Foa, P.P., Zak, B., 1967. Determination of phosphate - study of labile organic phosphate interference. Clin. Chim. Acta 15 (1), 155–&.

Barret, L.A., Barrot-Ivolot, C., Raynal, S., Jungas, C., Polidori, A., Bonnete, F., 2013a. Influence of hydrophobic micelle structure on crystallization of the photosynthetic RC-LH1-PufX complex from Rhodobacter blasticus. J. Phys. Chem. B 117 (29), 8770–8781.

Barret, L.A., Barrot-Ivolot, C., Raynal, S., Jungas, C., Polidori, A., Bonnete, F., 2013b. Influence of hydrophobic micelle structure on crystallization of the photosynthetic RC-LH1-PufX complex from rhodobacter blasticus. J. Phys. Chem. B 117 (29), 8770–8781.

Berman, H.M., Westbrook, J., Feng, Z., Gilliland, G., Bhat, T.N., Weissig, H., et al., 2000. The protein Data Bank. Nucleic Acids Res. 28 (1), 235–242.

Bjorkskov, F.B., Krabbe, S.L., Nurup, C.N., Missel, J.W., Spulber, M., Bomholt, J., et al., 2017a. Purification and functional comparison of nine human Aquaporins produced in Saccharomyces cerevisiae for the purpose of biophysical characterization. Sci. Rep. (U.K.) 7.

Bjorkskov, F.B., Krabbe, S.L., Nurup, C.N., Missel, J.W., Spulber, M., Bomholt, J., et al., 2017b. Purification and functional comparison of nine human Aquaporins produced in Saccharomyces cerevisiae for the purpose of biophysical characterization. Sci. Rep. 7 (1), 16899.

Breibeck, J., Rompel, A., 2019. Successful amphiphiles as the key to crystallization of membrane proteins: bridging theory and practice. Biochim. Biophys. Acta Gen. Subj. 1863 (2), 437–455.

Carlson, M.L., Young, J.W., Zhao, Z.Y., Fabre, L., Jun, D., Li, J.N., et al., 2018. The Peptidisc, a simple method for stabilizing membrane proteins in detergent-free solution. Elife 7.

Chae, P.S., Rasmussen, S.G.F., Rana, R.R., Gotfryd, K., Chandra, R., Goren, M.A., et al., 2010. Maltose-neopentyl glycol (MNG) amphiphiles for solubilization, stabilization and crystallization of membrane proteins. Nat. Methods 7 (12), 1003. U90.

Cheng, Y.F., 2015. Single-particle cryo-EM at crystallographic resolution. Cell 161 (3), 450–457.

Cheng, Y.F., 2018. Membrane protein structural biology in the era of single particle cryo-EM. Curr. Opin. Struct. Biol. 52, 58–63.

Cournia, Z., Allen, T.W., Andricioaei, I., Antonny, B., Baum, D., Brannigan, G., et al., 2015. Membrane protein structure, function, and dynamics: a perspective from experiments and theory. J. Membr. Biol. 248 (4), 611–640.

Denisov, I.G., Sligar, S.G., 2016. Nanodiscs for structural and functional studies of membrane proteins. Nat. Struct. Mol. Biol. 23 (6), 481–486.

Fuguet, E., Rafols, C., Roses, M., Bosch, E., 2005. Critical micelle concentration of surfactants in aqueous buffered and unbuffered systems. Anal. Chim. Acta 548 (1–2), 95–100.

Gotfryd, K., Mosca, A.F., Missel, J.W., Truelsen, S.F., Wang, K.T., Spulber, M., et al., 2018a. Human adipose glycerol flux is regulated by a pH gate in AQP10. Nat. Commun. 9.

Gotfryd, K., Mosca, A.F., Missel, J.W., Truelsen, S.F., Wang, K., Spulber, M., et al., 2018b. Human adipose glycerol flux is regulated by a pH gate in AQP10. Nat. Commun. 9 (1), 4749.

Gourdon, P., Liu, X.Y., Skjorringe, T., Morth, J.P., Moller, L.B., Pedersen, B.P., et al., 2011a. Crystal structure of a copper-transporting PIB-type ATPase. Nature 475 (7354), 59–U74.

Gourdon, P., Liu, X.Y., Skjorringe, T., Morth, J.P., Moller, L.B., Pedersen, B.P., et al., 2011b. Crystal structure of a copper-transporting PIB-type ATPase. Nature 475 (7354), 59–64.

Guillet, P., Mahler, F., Gamier, K., Boussambe, G.N.M., Igonet, S., Vargas, C., et al., 2019. Hydrogenated diglucose detergents for membrane-protein extraction and stabilization. Langmuir 35 (12), 4287–4295.

Hahn, A., Vonck, J., Mills, D.J., Meier, T., Kuhlbrandt, W., 2018. Structure, mechanism, and regulation of the chloroplast ATP synthase. Science 360 (6389).

Hong, W.X., Baker, K.A., Ma, X.Q., Stevens, R.C., Yeager, M., Zhang, Q.H., 2010. Design, synthesis, and properties of branch-chained maltoside detergents for stabilization and crystallization of integral membrane proteins: human connexin 26. Langmuir 26 (11), 8690–8696.

Hovers, J., Potschies, M., Polidori, A., Pucci, B., Raynal, S., Bonnete, F., et al., 2011. A class of mild surfactants that keep integral membrane proteins water-soluble for functional studies and crystallization. Mol. Membr. Biol. 28 (3), 170–180.

Junge, F., Schneider, B., Reckel, S., Schwarz, D., Dotsch, V., Bernhard, F., 2008. Large-scale production of functional membrane proteins. Cell. Mol. Life Sci. 65 (11), 1729–1755.

Kitchen, P., Salman, M.M., Halsey, A.M., Clarke-Bland, C., MacDonald, J.A., Ishida, H., et al., 2020. Targeting aquaporin-4 subcellular localization to treat central nervous system edema. Cell 181 (4), 784–799 e19.

Kotov, V., Bartels, K., Veith, K., Josts, I., Subhramanyam, U.K.T., Gunther, C., et al., 2019. High-throughput stability screening for detergent-solubilized membrane proteins. Sci. Rep. 9 (1), 10379.

Kotov, V, Mlynek, G, Vesper, O, Pletzer, M, Wald, J, Teixeira-Duarte, CM, Celia, H, Garcia-Alai, M, Nussberger, S, Buchanan, SK, Morais-Cabral, JH, Loew, C, Djinovic-Carugo, K, Marlovits, TC, 2021 Jan. In-depth interrogation of protein thermal unfolding data with MoltenProt. Protein Sci 30 (1), 201–217.

Kulandaisamy, A., Priya, S.B., Sakthivel, R., Frishman, D., Gromiha, M.M., 2019. Statistical analysis of disease-causing and neutral mutations in human membrane proteins. Proteins 87 (6), 452–466.

Lin, W., Chai, J., Love, J., Fu, D., 2010. Selective electrodiffusion of zinc ions in a Zrt-, Irt-like protein, ZIPB. J. Biol. Chem. 285 (50), 39013–39020.

Mineev, K.S., Nadezhdin, K.D., 2017. Membrane mimetics for solution NMR studies of membrane proteins. Nanotechnol. Rev. 6 (1), 15–32.

Mio, K., Sato, C., 2018. Lipid environment of membrane proteins in cryo-EM based structural analysis. Biophys. Rev. 10 (2), 307–316.

Moraes, I., Evans, G., Sanchez-Weatherby, J., Newstead, S., Stewart, P.D.S., 2014. Membrane protein structure determination the next generation. Biochim. Biophys. Acta Biomembr. 1838 (1), 78–87.

Padilla-Benavides, T., McCann, C.J., Arguello, J.M., 2013. The mechanism of Cu+ transport ATPases interaction with CU+ chaperones and the role OF transient METAL-BINDING sites. J. Biol. Chem. 288 (1), 69–78.

Pandey, A., Shin, K., Patterson, R.E., Liu, X.Q., Rainey, J.K., 2016. Current strategies for protein production and purification enabling membrane protein structural biology. Biochem. Cell. Biol. 94 (6), 507–527.

Parker, J.L., Newstead, S., 2012. Current trends in alpha-helical membrane protein crystallization: an update. Protein Sci. 21 (9), 1358–1365.

Pedersen, P.A., Rasmussen, P.L., Joorgensen, P.L., 1996. Expression in high yield of pig alpha 1 beta 1 Na,K-ATPase and inactive mutants D369N and D807N in Saccharomyces cerevisiae. J. Biol. Chem. 271 (5), 2514–2522.

Popot, J.L., 2010. Amphipols, nanodiscs, and fluorinated surfactants: three nonconventional approaches to studying membrane proteins in aqueous solutions. Annu. Rev. Biochem. 79, 737–775.

Prive, G.G., 2007. Detergents for the stabilization and crystallization of membrane proteins. Methods 41 (4), 388–397.

Seddon, A.M., Curnow, P., Booth, P.J., 2004. Membrane proteins, lipids and detergents: not just a soap opera. Biochim. Biophys. Acta Biomembr. 1666 (1–2), 105–117.

Sim, D.W., Lu, Z., Won, H.S., Lee, S.N., Seo, M.D., Lee, B.J., et al., 2017. Application of solution NMR to structural studies on alpha-helical integral membrane proteins. Molecules 22 (8).

Slotboom, D.J., Duurkens, R.H., Olieman, K., Erkens, G.B., 2008. Static light scattering to characterize membrane proteins in detergent solution. Methods 46 (2), 73–82.

Sorensen, T.L.M., Moller, J.V., Nissen, P., 2004. Phosphoryl transfer and calcium ion occlusion in the calcium pump. Science 304 (5677), 1672–1675.

Sousa, J.S., Mills, D.J., Vonck, J., Kuhlbrandt, W., 2016. Functional asymmetry and electron flow in the bovine respirasome. Elife 5.

Stetsenko, A., Guskov, A., 2017. An overview of the top ten detergents used for membrane protein crystallization. Crystals 7 (7).

Strop, P., Brunger, A.T., 2005. Refractive index-based determination of detergent concentration and its application to the study of membrane proteins. Protein Sci. 14 (8), 2207–2211.

Stroud, Z., Hall, S.C.L., Dafforn, T.R., 2018. Purification of membrane proteins free from conventional detergents: SMA, new polymers, new opportunities and new insights. Methods 147, 106–117.

Tate, C.G., 2010. Practical considerations of membrane protein instability during purification and crystallisation. Methods Mol. Biol. 601, 187–203.

Thonghin, N., Kargas, V., Clews, J., Ford, R.C., 2018. Cryo-electron microscopy of membrane proteins. Methods 147, 176–186.

Tiefenauer, L., Demarche, S., 2012. Challenges in the development of functional assays of membrane proteins. Materials 5 (11), 2205–2242.

Toyoshima, C., Nakasako, M., Nomura, H., Ogawa, H., 2000. Crystal structure of the calcium pump of sarcoplasmic reticulum at 2.6 angstrom resolution. Nature 405 (6787), 647–655.

UniProt, C., 2019. UniProt: a worldwide hub of protein knowledge. Nucleic Acids Res. 47 (D1), D506–D515.

Wu, D., Grund, T.N., Welsch, S., Mills, D.J., Michel, M., Safarian, S., et al., 2020. Structural basis for amino acid exchange by a human heteromeric amino acid transporter. Proc. Natl. Acad. Sci. U. S. A. 117 (35), 21281–21287.

Zhang, T., Liu, J., Fellner, M., Zhang, C., Sui, D.X., Hu, J., 2017. Crystal structures of a ZIP zinc transporter reveal a binuclear metal center in the transport pathway. Sci. Adv. 3 (8), e1700344.